Surface Sciences 47 (1975) 384–402

THERMAL DESORPTION FROM METAL SURFACES: A REVIEW

David A. KING *
School of Chemical Sciences, University of East Anglia, Norwich, NOR 88C, England

In this review an attempt is made to draw correlations between thermal desorption and structural studies of chemisorption on metal surfaces. Alternative models are discussed for the appearance of multiple peaks and for lineshape analysis in desorption, the first involving multiple binding states and the second lateral interactions within a homogeneous chemisorbed layer. Criteria are discussed for distinguishing between the various possibilities for a particular system, in particular with relation to the adsorption of hydrogen and carbon monoxide on tungsten.

1. Introduction

The temperature-programmed thermal desorption ("flash filament") technique, first described by Apker [1], has been increasingly used since the late 1950's to characterise the energetics and surface stoichiometry for absorbate on polycrystalline wires and ribbons [2–4], and, more recently, on single crystal planes. Since adsorption on clean metal surfaces is generally a non-activated process, the desorption activation energy E is approximately equal to the differential heat of adsorption. The technique is thus, at first sight, the simplest method available for obtaining a measure of the bond energy in adsorption; calorimetric or isosteric heat measurements are more reliable, but more tedious. In addition, the reaction order for desorption may, under favourable circumstances, be deduced from a family of desorption traces obtained at different initial coverages; this information can provide a pointer to the dissociative or non-dissociative state of the adsorbate. Where the vacuum system volume and pumping speed have been measured, and the latter is reliably constant, the technique also provides a quantitative measure of the amount of adsorbate present on the surface prior to the flash. However, the detailed interpretation of desorption traces is seldom unambiguous, particularly in the absence of complimentary structural data. We shall see that the analysis of the data is itself dependent on the structural model assumed for the adsorbed layer.

Experimentally, a temperature program, preferably linear in time, is applied to the adsorbent after adsorption at a given temperature, and the pressure in the continuously pumped system is recorded, producing a desorption trace. The rate of

* Present address: The Donnan Laboratories, The University, Liverpool, England.

desorption per unit area of adsorbent is calculated from the expression

$$dN/dt = (V/AkT_g)\,[dP/dt + (S/V)P]\,, \tag{1}$$

where N is the surface coverage (molecule cm^{-2}); P is the pressure increase above the background; V is the volume of the desorption chamber; S is the system pumping speed; A is the adsorbent area; and T_g is the gas phase temperature. If the pumping speed to volume ratio is large and the heating rate $dT/dt\,(=\beta)$ is low, $dP/dt \ll (S/V)P$, and the desorption rate is conveniently proportional to the pressure increase P.

Major experimental pitfalls, all of which tend to broaden the desorption trace halfwidth and thus render lineshape analysis hazardous, if not useless, are: temperature inhomogeneity across the adsorbent during the flash, the most common cause being the cooling effect of heavy support rods; desorption from the support rods themselves (one of the peaks in a three-peak trace for H_2 on W{211} [5] has been attributed [6] to such an effect); and reversible adsorption–desorption effects occurring at the reaction vessel walls. A further difficulty may arise where interconversion from one state of adsorbate (e.g. molecular) to another (e.g. atomic) occurs during the flash: except where the adlayer is fully equilibrated, desorption traces may not reflect the adsorbate distribution pertaining prior to the flash. Finally, if slow heating rates and pumping speeds are employed, re-adsorption during a flash may become appreciable. For example, if the pressure during desorption rises to $\sim 10^{-7}$ torr ($\sim 10^{-9}$ Pa), the heating rate should be 50 K s^{-1} or higher if this problem is to be avoided.

Complex desorption traces, consisting of multiple peaks and shoulders, have been traditionally interpreted in terms of a set of physically and chemically distinct "binding states" (e.g. γ-nitrogen, a molecular species, and β-nitrogen, an atomic species, on tungsten [2]), each having a characteristic desorption activation energy [2,3]. Multiple peaks observed from polycrystalline adsorbents were often attributed to desorption of species from different crystal planes. However, even on homogeneous single crystal adsorbents single peaks are the exception rather than the rule, and recently it has been shown [7–9] that complex traces may arise from repulsive lateral interactions between adsorbed species where, in contrast to the multi-state model, the entire adsorbed layer is homogeneous at all coverages. The two models require different analytical procedures.

2. Desorption trace analysis: Polanyi–Wigner model

In the Polanyi–Wigner model it is assumed that the rate of desorption from a species in state i on a surface may be written in the form

$$-dN_i/dt = \nu_i N_i^{x_i} \exp(-E_i/RT)\,, \tag{2}$$

where x_i is the reaction order for desorption from state i, ν_i is a frequency factor,

E_i is the desorption activation energy and N_i is the population (molecule cm^{-2}) in state i. A variety of methods are available for deducing values for these parameters from the experimental data.

2.1. Redhead's desorption peak temperature method

When the pumping speed and heating rate are such that the desorption rate is proportional to the pressure (see section 1), Redhead [3] showed that for first order desorption ($x_i = 1$) the activation energy for desorption E_i is approximately related to the temperature T_{pi} at which a peak occurs in the desorption trace through the expression

$$E_i = RT_{pi}\,[\ln(\nu_i\, T_{pi}/\beta) - 3.46]\,, \tag{3}$$

where β ($= dT/dt$) is the heating rate. Fig. 1 shows Redhead's plot of E as a function of T_p for $\nu = 10^{13}$ sec^{-1} and β between 1 and 1000 K sec^{-1}, and gives a very simple method of obtaining estimates of E_i from a desorption trace. It does, however, depend on a guess at ν.

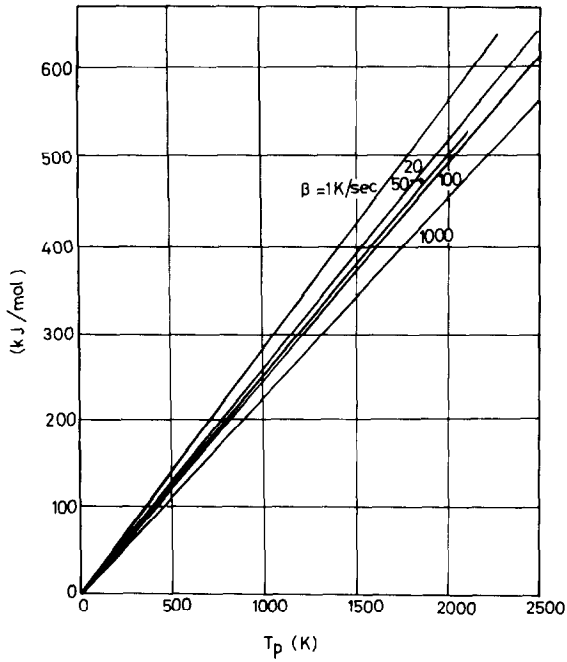

Fig. 1. Variation of desorption trace peak temperature T_p with desorption activation energy E, for first order desorption assuming $\nu = 10^{13}$ sec^{-1}. Reproduced from Redhead [3], with permission.

Provided that E is independent of coverage, when the desorption process is first order, T_{pi} is independent of coverage. For second order desorption, T_{pi} decreases with increasing coverage, but even here fig. 1 is a useful guide to E_i if the peak temperature is taken from a low coverage desorption trace. Even for first order desorption, however, this method is approximate, relying as it does on the assumptions of a reasonable value for ν_i and the independence of ν_i and E_i on coverage. Only a complete lineshape analysis of the desorption traces can yield accurate values for the desorption rate parameters, and even then ambiguities can seldom be entirely eliminated.

2.2. Lineshape analysis: single-peak desorption traces

(i) "Complete" analysis. Here we do not make the assumption that ν and E are independent of coverage. For a single state, the rate equation is simply

$$-\mathrm{d}N/\mathrm{d}t = \nu(N)N^x \exp[-E(N)/RT]\,. \tag{4}$$

$E(N)$ is evaluated first. From eq. (1), assuming, for simplicity, that $\mathrm{d}P/\mathrm{d}t \ll (S/V)P$, the coverage at a time t after starting the sweep is given by

$$N_t = S/(AkT_g)\int_t^\infty P\,\mathrm{d}t\,. \tag{5}$$

From a family of desorption traces corresponding to different initial coverages, eq. (5) is used to construct a family of curves of N_t as a function of t; for a given value of N_t, several values of t, corresponding to a range of values of the temperature of the adsorbent T, can be obtained, and, since the desorption rate for each combination of N_t and T is known from the desorption trace [using eq. (1)], an Arrhenius plot of ln rate against $1/T$ can be constructed corresponding to the constant coverage N_t. Since the pre-exponential is constant at constant N, the slope yields $E(N)$ at N_t, independent of the value of ν or x. Repeating this for different values of N_t, a plot of $E(N)$ as a function of N can be constructed. The intercepts on the Arrhenius plots yield $\ln\nu(N) + x\ln N$; thus, if the plot of intercept against $\ln N$ is linear, ν is coverage-independent and is given by the intercept, and x is unambiguously given by the slope. If this plot is non-linear, integral values of x must be tried to determine $\nu(N)$, which leads to possible ambiguities. This analytical method has been applied, for example, to the WO_3 (1700) desorption trace from oxygen on tungsten by King, Madey and Yates [10].

(ii) Computer fitting. A more commonly employed procedure [11,12] is to compute desorption traces from eq. (4), assuming that ν and E are coverage-independent, finally producing a best-fit curve to the experimental data for a set of values of x, ν and E. This procedure was applied, for example, to the analysis of desorption traces from xenon on W{111} [13], best-fits being generated for $\nu = 10^{15}\ \mathrm{sec}^{-1}$, $x = 1$ and a variable E at low coverages tending to a constant value of 39 kJ mol^{-1} at frac-

tional coverages $\theta > 0.07$. This procedure is not entirely self-consistent, as each desorption trace for a given initial coverage is computed on the assumption of a coverage-independent E.

(iii) An alternative method, outlined by Redhead [3] and discussed in detail by Lord and Kittelberger [14], is to compare desorption traces obtained with widely different experimental heating rates, β. The slope of $\ln(T_p^2/\beta)$ against $1/T_p$ reproduces E for both first and second order desorption. As indicated in fig. 1, T_p is not very sensitive to β, so that accurate data are required over at least an order of magnitude change in β for this method to be reliable. Furthermore, the assumption is made here that both ν and E are coverage independent.

2.3. Lineshape analysis: multiple peak traces

The simplest, and most commonly employed, method is to resolve the desorption trace into component monotonic curves on the basis of the structural features of the trace, deduce the order of desorption for each state from the behaviour of T_p with coverage, and, assuming a value for ν, to make use of fig. 1 to obtain estimates for E for each state.

More sophisticated lineshape analytical procedures have been developed. Thus, Winterbottom [15,16] utilizes the following expression for the rate of desorption from binding state i:

$$dN_i/dt = \nu_i N_i^{x_i} \exp(-E_i/RT) + s_i P(2\pi mkT_g)^{-1/2} + F_i\,, \tag{6}$$

which takes account of the rate of readsorption, s_i being the sticking probability for the ith state, and F_i is the net interconversion of other binding states to or from state i during the flash. The total rate of desorption, obtained from the experimental desorption trace through eq. (1), is given by

$$dN/dt = \sum_i dN_i/dt\,.$$

The detailed analytical procedure involves use of low, medium and high coverage desorption traces to resolve the trace into its i components, making use of the fact that preferential filling occurs at low coverages of states with the highest activation energies E_i. Best-fit values for ν, x and E pertaining to each binding state are finally extracted from the data.

A timely and important warning concerning the validity of results obtained by these procedures has recently been issued by Pisani, Rabino and Ricca [17]. Using a procedure essentially similar to the above, they report a detailed statistical examination of the application of two alternative models to desorption traces for nitrogen chemisorbed on polycrystalline tungsten. Figs. 2 (a) and 2 (b) show the results of their lineshape analysis of a single desorption trace. In both cases a two-state, β_1 and β_2, model is assumed. For the analysis presented in fig. 2 (a), it was assumed that the β_2 state desorbs with second order kinetics, and the β_1 with first order kinetics;

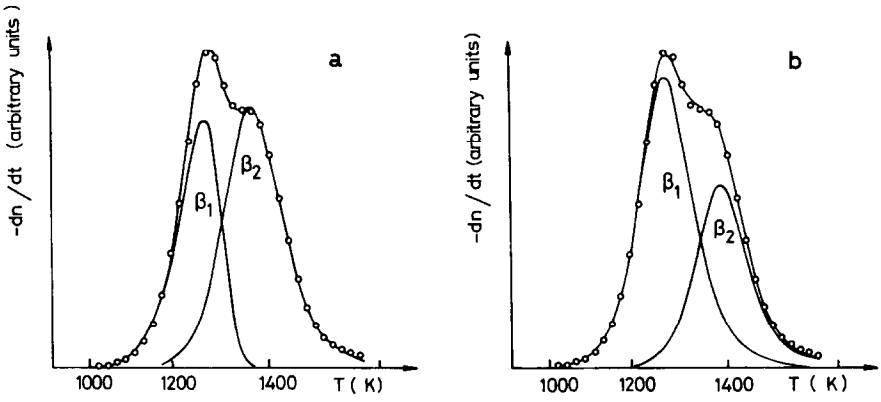

Fig. 2. Fit of a desorption trace from nitrogen on polycrystalline tungsten according to two multi-state models. Points indicate experimental data after an exposure of 5×10^{-3} Pa sec at 800 K. Heavy lines are best fitting curves and light lines define the component β_1 and β_2 peaks according to (a) first order desorption for β_1, second order for β_2; and (b) second order for both states. Reproduced from Pisani, Rabino and Ricca [17], with permission.

while for fig. 2(b) both were assumed to desorb with second order kinetics. No choice was possible between the two models, for which statistical calculations indicated equivalent standard deviations from the experimental data. Further, for their analyses illustrated here, the authors made the arbitrary assumptions that ν_i and E_i were independent of θ_i for each state; if these were dropped, a wide range of these parameters could be found to produce equally good "best-fit" curves. One is thus forced to the conclusion that the analysis of complex desorption traces is necessarily fraught with ambiguities, even within the framework of the simple multistate model.

3. Desorption trace analysis: interaction model [7–9]

The existence of indirect or direct lateral interactions between chemisorbed species on single crystal surfaces may be inferred from the abundance of LEED data accrued over the past decade or more, in which ordered structures have been observed in the overlayer at submonolayer coverages. For example, double-spaced structures observed for N_2, CO and H_2 on a variety of tungsten single crystal planes imply repulsive interaction between nearest neighbours. Other data have also been interpreted in terms of lateral interactions: thus, in fig. 3 desorption traces from Yates and Madey [16] are shown for H_2 from a W{100} surface with increasing amounts of coadsorbed CO (the CO being adsorbed after H_2). The β_2 and β_1 "states" observed in the absence of CO are gradually converted into a new set of

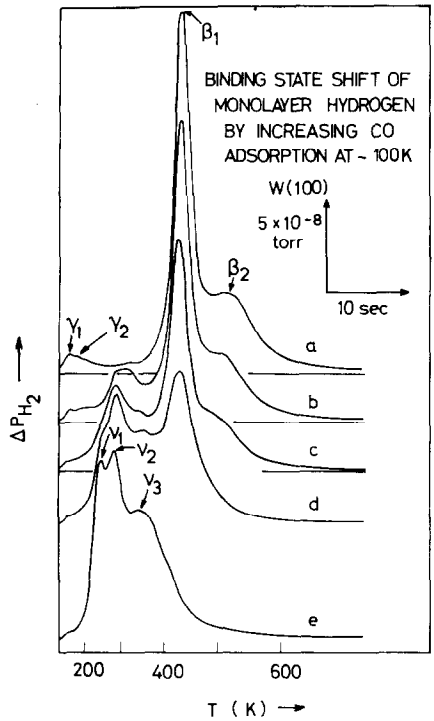

Fig. 3. Desorption traces for H_2 from W{100} with coadsorbed CO. Trace (a), no CO; (b)–(e), increasing exposures to CO after H_2 adsorption at 100 K. Reproduced from Yates and Madey [18], with permission.

"states", ν_1, ν_2 and ν_3; the implied lowering of the desorption activation energy for hydrogen is attributed to absorbate–adsorbate interactions.

The theoretical basis for indirect interactions between adatoms, involving electron-sharing through the substrate metal electron band and exhibiting oscillatory and anisotropic behaviour, has been developed by Grimley [19,20] and by Einstein and Schrieffer [21], and more recently by Grimley and Torrini [22] for substrate–atom-sharing interactions.

Over 30 years ago, Roberts and coworkers [23] examined some of the implications of lateral interactions (then erroneously believed to arise from through-space dipole–dipole interactions) for adsorption and desorption kinetics. An important feature of the model was developed by Wang [24,25] who showed that on a surface mesh exhibiting four-fold symmetry and with lateral repulsive interactions between nearest neighbour adatoms, the adsorption heat falls sharply at a half monolayer coverage. The assumptions of the model are as follows:

(1) At all coverages, adsorption occurs on specific surface sites, and all sites are equivalent.

(2) The pairwise nearest neighbour interaction energy is ω; all other lateral interactions are ignored.
(3) The distribution of adsorbate on sites corresponds to the thermodynamic (equilibrium) distribution.
(4) A site is either occupied or unoccupied; multilayer adsorption or adsorbate penetration into the bulk are precluded.
(5) The interaction energy ω is assumed to be independent of coverage.

3.1. Non-dissociative adsorption

For non-dissociative adsorption, the model yields the following expression [24] for the differential energy of adsorption as a function of θ:

$$U_g - \bar{U}_s = (U_g - U_s)_0 + \tfrac{1}{2} z\omega \left[1 - \frac{1-2\theta}{[1-4\theta(1-\theta)(1-\exp(\omega/RT))]^{1/2}} \right], \quad (7)$$

where $(U_g - U_s)_0$ is the adsorption energy at $\theta = 0$ and z is the number of nearest neighbour (n.n.) sites. In the limit where $\omega/T \to 0$, i.e. at temperatures sufficiently high for the adlayer to be disordered, the right-hand side of eq. (7) reduces to

$$(U_g - U_s)_0 + z\omega\theta ,$$

i.e. there is a linear dependence of adsorption energy on θ. When $\omega/T \to -\infty$, however, there are two limits: at $\theta \leqslant 0.5$, $(U_g - \bar{U}_s) = (U_g - U_s)_0$; and at $\theta \geqslant 0.5$, $U_g - \bar{U}_s = (U_g - U_s)_0 + z\omega$. In this case there is a discontinuous change in the adsorption energy at $\theta = 0.5$. Following the conceptually simple formulation of Goymour and King [8], the desorption rate is written as

$$-\frac{dN}{dT} = K \frac{kT}{h} N \frac{f^{\neq}}{f_N} \exp -\left(\frac{E}{RT}\right), \quad (8)$$

where K is a transmission coefficient, and $f^{\neq}$ and f_N are partition functions for the activated complex and filled sites, respectively. E is then equated to the differential adsorption energy given by eq. (7). (Adams [9], following Roberts [23], does not make this assumption. This detail has been discussed in ref. 8: here we point out that if adsorption is nonactivated for all θ, as shown for a number of systems, it will be a good approximation.) Fig. 4 illustrates the effect of the repulsive interaction energy ω on the computed desorption traces, illustrating clearly the separation of the peak into a doublet with theoretically reasonable values of ω [21,22].

It is worth noting that eq. (8) has the same form as eq. (4), with $x = 1$. Thus, for nondissociative adsorption the "complete" analytical procedure described in section 2.2 (i) can be used to empirically derive the functional dependence of E on coverage [eq. (7)] from experimental desorption traces exhibiting multiple peaks, in cases where the interaction model is structurally appropriate.

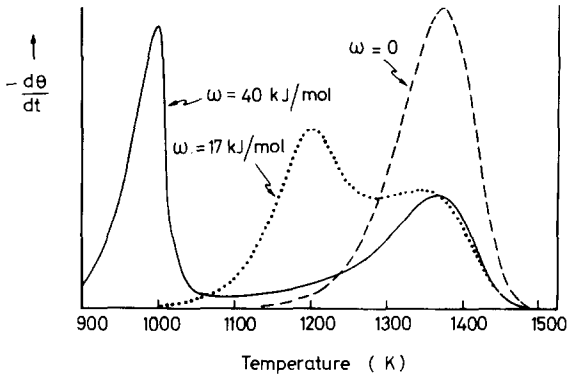

Fig. 4. Variation of computed desorption traces with nearest neighbour repulsive interaction energy ω, for first order desorption with E_0 = 318 kJ mol^{-1}. Reproduced from D.L. Adams [9], with permission.

3.2. Dissociative adsorption

For the dissociative adsorption of a homonuclear diatomic molecule A_2 on a two- or four-fold symmetric lattice, the model yields a similar expression to eq. (7):

$$U_g - \bar{U}_s = (U_g - U_s)_0 + z\omega \left[1 - \frac{1 - 2\theta}{[1 - 4\theta(1-\theta)(1 - \exp(\omega/RT))]^{1/2}} \right]. \quad (9)$$

The desorption rate is now

$$-\frac{dN}{dt} = K \frac{kT}{h} N_{AA} \frac{f^{\neq}}{f_{AA}} \exp\left(-\frac{E}{RT}\right), \quad (10)$$

where N_{AA} is the coverage in nearest neighbour occupied site pairs on the surface, and f_{AA} is the partition function for these occupied site pairs. The assumption is made in writing (10) that n.n. sites must be occupied for the desorption activated complex to be formed. E is equated to $U_g - \bar{U}_s$, and two-dimensional lattice statistics yield the following expression for N_{AA}:

$$N_{AA} = \tfrac{1}{4} z N_s \left[\theta - \frac{2\theta(1-\theta)}{[1 - 4\theta(1-\theta)(1 - \exp(\omega/RT))]^{1/2} + 1} \right] \quad (11)$$

where N_s is the number of sites cm^{-2}. Here, we note that the pre-exponential in eq. (10) does not have the simple form of the Polanyi–Wigner equation, and the analytical procedure described in section 2.2 (i) can no longer be employed, although the functional dependence of E on θ can be extracted by that procedure. Data are usually analysed by computing desorption traces from eq. (10), varying the parameters $Kf^{\neq}/f_{AA}$, the interaction energy ω (negative when repulsive) and the activation

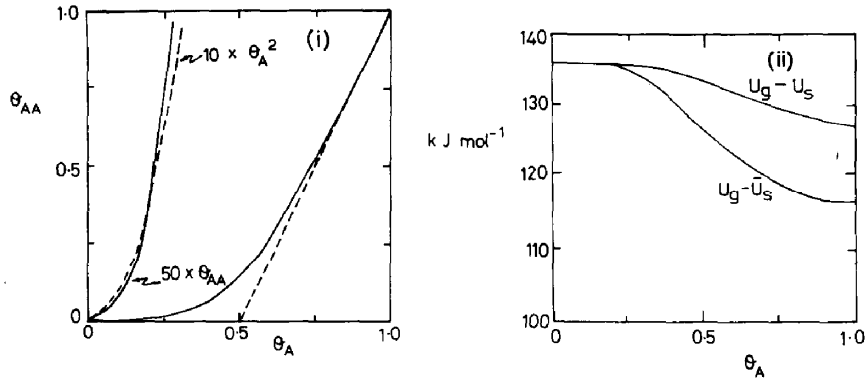

Fig. 5. Dependence of $U_g - \bar{U}_s$ and θ_{AA} [eqs. (9) and (11)] on θ for a one-dimensional lattice ($Z = 2$) with a repulsive n.n. interaction energy of 4.18 kJ mol^{-1} and $(U_g - U_s)_0 = 135$ kJ mol^{-1}, at 400 K.

energy for desorption at zero coverage, E_0 ($= (U_g - U_s)_0$), to obtain a best-fit to the experimental data.

Fig. 5 illustrates the variation of $U_g - \bar{U}_s$ and θ_{AA} ($= N_{AA}/\frac{1}{4} z N_s$) with fractional coverage θ for a lattice with $z = 2$ and $\omega = 4.18$ kJ mol^{-1}. At low coverages, θ_{AA} approximates to a θ^2 dependence; while at high coverages θ_{AA} is almost a linear function of θ, producing pseudo-first order kinetics – even where the adsorption is dissociative. For intermediate values of ω/T, however, $U_g - \bar{U}_s$ is not constant at $\theta > 0.5$ and the peak temperature will shift downwards with increasing coverage, imitating second-order behaviour. This will, of course, also hold for nondissociative adsorption, and for this reason, as pointed out by Adams, it may be difficult to distinguish dissociative from nondissociative adsorption. Again, therefore, ambiguities are not easily eliminated.

The analysis has been extended to include the dissociative adsorption of a heteronuclear diatomic [8], and can be developed for any crystallographic symmetry, or to include next nearest neighbour interactions, using, for example, the order–disorder formalism developed by Hijmans and De Boer [26]. In principle at least, more complex desorption traces may therefore be tackled; this is a fruitful possibility where structural studies indicate the applicability of the model. Finally, we note that the lateral interaction model has also been applied to the study of *adsorption* kinetics on single crystal surfaces [27].

4. Desorption activation energies and "binding energies"

The term "binding energy" is widely used in relation to desorption activation energies or differential energies of adsorption. Here we interpose a brief note on the

use of this term in relation to the two models, multistate and lateral interaction, described above. We consider an example where two peaks, labelled α and β, are observed in the desorption spectra; β is associated with the higher value of E. For simplicity, we suppose both species to be non-dissociatively adsorbed; in this case the "binding energy" is simply $U_g - U_s$, where U_g is the system energy with the species in the gas phase and U_s is the energy with the species adsorbed on the surface.

We consider first the two-state model; at high coverages both α and β states coexist on the surface as energetically distinct species. At low coverages, i.e. below the saturation coverage θ_β in the β state, in an equilibrated adlayer most of the adsorbate will be in the β state. Thus we can write for the β state "binding energy":

$$(U_g - U_s)_\beta = \frac{1}{\theta} \int_0^{\theta_\beta} (U_g - \bar{U}_s)\, d\theta \,. \tag{12}$$

As pointed out above, the differential adsorption energy $U_g - \bar{U}_s$ is the experimentally determined quantity, which we have equated to E. Similarly, since α adsorption dominates above θ_β, the α state "binding energy" is given by:

$$(U_g - U_s)_\alpha = \frac{1}{\theta - \theta_\beta} \int_{\theta_\beta}^{1} (U_g - \bar{U}_s)\, d\theta \,. \tag{13}$$

Clearly, in this model each state has a distinct "binding energy"; provided the differential energy is not strongly θ-dependent in each state, the "binding energies" are approximately equal to the differential energies. For the lateral interaction model, however, the adlayer is homogeneous at all coverages. Thus the "binding energy" at any coverage θ is simply

$$U_g - U_s = \frac{1}{\theta} \int_0^{\theta} (U_g - \bar{U}_s)\, d\theta \,. \tag{14}$$

In fig. 5 (ii) the function $U_g - U_s$ has been determined for the lateral interaction model. This illustrates the simple fact that here the "binding energy" at high coverages is significantly higher than the experimentally determined differential energy. In our view the term "binding energy" is misleading, and should be avoided.

5. Adsorption systems

This section is intended to be illustrative, not exhaustive; a very lengthy article would result from any attempt at the latter. A few topical adsorption systems have been selected, to illustrate the main theme of this review, that desorption kinetic parameters cannot be extracted from thermal desorption data without a full understanding of the adlayer structure.

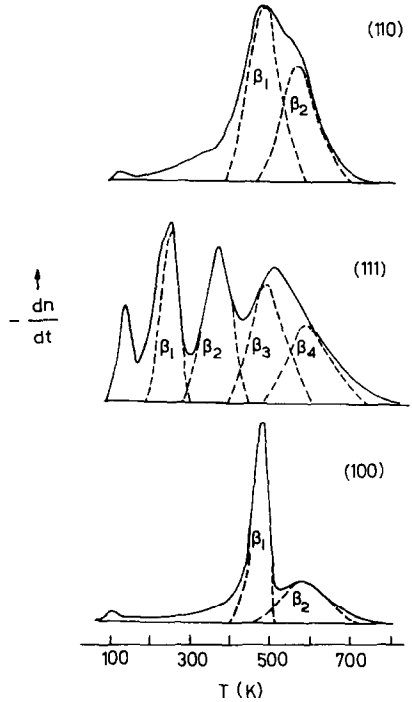

Fig. 6. Desorption traces for hydrogen on W{100}, {110} and {111} crystal planes corresponding to saturation of the surface. Reproduced from Tamm and Schmidt [28], with permission.

5.1. Hydrogen on tungsten

Desorption traces for H_2 on {100}, {110} and {111} crystal planes [28] are illustrated in fig. 6, clearly demonstrating crystallographic anisotropy in desorption kinetics. The low peak-temperature γ states, which do not exhibit isotopic exchange with D_2, are distinct, molecular binding states; our attention is directed at the origin of the multiple peaks observed in the β states.

5.1.1. H_2 on W{110}

The saturation coverage is reported [29] as 14×10^{14} H atom cm^{-2}, which is close to the number (14.2×10^{14} cm^{-2}) of W atoms in this close-packed plane. Two β peaks are observed (β_1 and β_2), and the two-state model yields equal saturation coverages in each state, second order kinetics for both, and respective desorption energies of 113 and 138 kJ mol^{-1}. A RHEED study [30] revealed that hydrogen adsorption proceeds with the formation of a (2×1) structure, presumably corresponding to $\theta = 0.5$. Photoelectron spectra [31] show low coverage energy levels at

0.3, 2.2, 2.6, 3.8 and 6.5 eV below the Fermi level; at high coverages the −2.6 eV level shifts to −3.5 eV, and the −6.5 eV level drops to −7.2 eV. These data favour the interaction model: a two-state model would require the *addition* of new levels to the low coverage spectra. Finally, an electron stimulated desorption study [32] has been reported for this system. The H^+ desorption cross section at half a monolayer is about 30% less than that for monolayer coverage, again consistent with the lateral interaction model. At this stage, therefore, all the data are consistent with this model, which yields a nearest neighbour interaction energy of $\sim 6\,\mathrm{kJ\,mol^{-1}}$. This is subject to a simple experimental test. The two-dimensional Ising model for order–disorder transitions yields the following relationship [33] between the critical temperature T_c and the interaction energy ω:

$$\exp(\omega/2kT_c) = 0.4142\ .$$

With $\omega = -6\,\mathrm{kJ\,mol^{-1}}$, we have $T_c = 415\,\mathrm{K}$; the half-monolayer (2 × 1) structure should therefore disappear when the substrate is heated to this temperature.

5.1.2. H_2 on W{100}

This system has been extensively studied in recent years. Desorption traces, reported by several authors [28,34], again show two β peaks, β_1 and β_2 (fig. 6), which, subjected to a two-state analysis, reveals first order kinetics for β_1 and second order for β_2, with respective desorption energies of $135\,\mathrm{kJ\,mol^{-1}}$ and $106\,\mathrm{kJ\,mol^{-1}}$. At saturation, there are two H adatoms per W atom in the {100} surface [29], and the saturation population ratio in the two states is $\beta_1 : \beta_2 = 2:1$. Originally, the data were interpreted in terms of a molecular β_1 state coadsorbed at high coverage with an atomic β_2 state [35], although this model was received with some scepticism [34]. Data obtained by a wide variety of techniques for this system are summarized below.

(i) Coadsorption studies with H_2 and D_2 revealed that both states were isotopically mixed on desorption [34]; the simplest interpretation is that the entire chemisorbed layer is composed of H adatoms at all coverages.

(ii) Within experimental error, the work function varies linearly with coverage up to saturation [34], with no break at $\frac{1}{3}$ of a monolayer as expected if the two states were distinct species.

(iii) Propst and Piper [36] studied the system by electron energy loss spectroscopy and report a major band at $1130\,\mathrm{cm^{-1}}$, corresponding to a W–H stretch, but no band in the region of $4000\,\mathrm{cm^{-1}}$ which could be attributed to an H–H stretch.

(iv) Plummer and Bell [37] showed that the field emission energy distribution technique was capable of producing vibrational spectra – the inelastic tunneling spectrum – and observed a band at $4430\,\mathrm{cm^{-1}}$ (550 eV) due to the H–H stretch for the low temperature γ state of H_2 on W{111}. However, no band attributable to an H–H stretch was found for hydrogen in the β state on W{100}.

(v) Several diffraction studies, LEED [38,39] and RHEED [40], have been reported for this system. As hydrogen adsorption proceeds, on the clean crystal, extra diffrac-

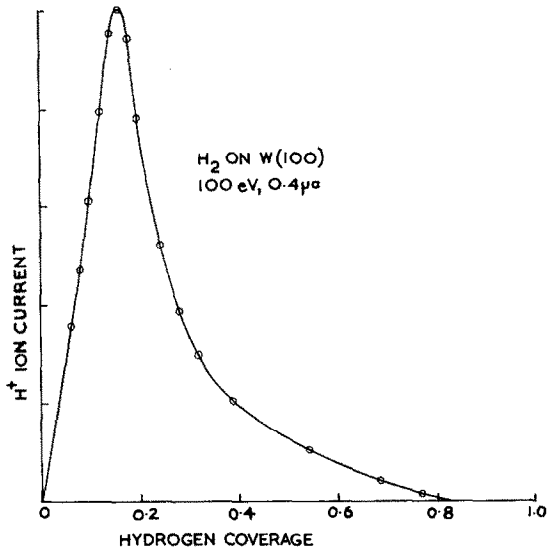

Fig. 7. Electron stimulated desorption of H^+ from hydrogen adsorbed on W{100} as a function of hydrogen coverage. Reproduced from Madey [29], with permission.

tion spots appear at the $\frac{1}{2}, \frac{1}{2}$ positions; these are most intense and sharp at ~0.2 of a monolayer, being ascribed to the formation of a c(2 X 2) structure in the adlayer. With further adsorption, the diffraction patterns become more complex, with each half order spot splitting into four new spots and decreasing in intensity; at ~0.35 of a monolayer the half order beams are completely attenuated, and the pattern during the remainder of the hydrogen uptake is similar to that for clean W{100}.

(vi) Madey [29] has examined the electron stimulated desorption (ESD) characteristics of hydrogen on W{100} as a function of coverage; his remarkable results are shown in fig. 7. At coverages where the c(2 X 2) structure is observed, the H^+ ion cross section is 1.8×10^{-23} cm^2, while at full coverage the cross section is $\ll 10^{-25}$ cm^2. While the results are clearly inconsistent with the two-state model, the ESD behaviour on this plane is quite different from that on the {110} [32], discussed above, and points to a more dramatic change in the adlayer at $\theta > 0.2$ than the simple incurrence of lateral interactions.

In summary, the results obtained for this plane present a strong case against the two-state model. However, as pointed out by Adams [9], the simple lateral interaction model predicts a population ratio of 1:1 for the two β peaks, whereas the experimental figure is 2:1. Furthermore, the model would imply a saturation coverage of 10×10^{14} H atom cm^{-2}, just half the experimental figure. Evidently a more complex model needs to be invoked for this system, possibly involving the changeover from one type of site to another for the entire adlayer as adsorption proceeds beyond

the c(2 × 2) structure. A quantitative description of the desorption traces for this system must clearly await a complete structural analysis, at both low and high coverages.

5.1.3. H_2 on W{111}

Other than desorption traces (fig. 6), few studies have been reported for H_2 on W{111}. Similar traces were obtained by Tamm and Schmidt [28] and by Madey [43]; there are four β peaks with desorption energies of 142, 115, 87 and 55 kJ mol^{-1}. The population ratios are 1:1.7:1.5:1, and at saturation there are two H adatoms to every *exposed* W atom in the rather open {111} plane. We note that the lateral interaction model for a hexagonal lattice would entail three equally populated peaks [23]; no simple interpretation can therefore be forwarded. The experimental data for this plane should, however, be treated with caution. King and Wells [44] suggest that there are as many as 10^{14} disordered tungsten atom cm^{-2} on a {111} plane of tungsten thermally annealed at 2500 K, so that an analysis based on a perfect {111} plane would necessarily be in error. This estimate was based on field ion micrographs from thermally annealed tips, which indicate a far more perfect atomic arrangement on the {100} and {110} planes.

5.2. Carbon monoxide on tungsten

Extensive investigations, reviewed by Ford [45] and in recent papers [46–49], have shown this to be a very complex system which is, as yet, incompletely understood. Here we simply draw attention to several details which are relevant to our theme. Desorption traces from a tungsten ribbon, basically {100}-oriented, are illustrated in fig. 8 [50]; more complex spectra have been reported [16]. After saturation at room temperature, there are three dominant peaks, labelled α, β_1 and β_2. The β_2 exhibits second order behaviour, while the β_1 and α exhibit first order behaviour. After adsorption at 100 K, a further state, the so-called "virgin" state, has been identified; this state does not desorb on heating, but undergoes a conversion to α and β states. Evidence, discussed below, indicates clearly that virgin, α and β states are, indeed, physically distinct species which co-adsorb at high coverages, while the β_1 and β_2 peaks are attributable to the lateral interaction model. In this case, therefore, we have a combination of multi-state and interaction models in one system.

The α state is itself composed of two sub-states, both non-dissociatively adsorbed. The molecular nature of this state was first demonstrated by its inability to undergo isotopic mixing, in contrast to the β states [51]. The two sub-states were revealed by electron stimulated desorption [52,53] and infrared reflection–absorption spectroscopy [54], the latter also confirming the molecular nature of these species; a resolution of the two α sub-states by thermal desorption has recently been reported [55].

Goymour and King [50] have reviewed the evidence for the β state on tungsten, and conclude that it is probably dissociatively adsorbed. More recently, a pertinent

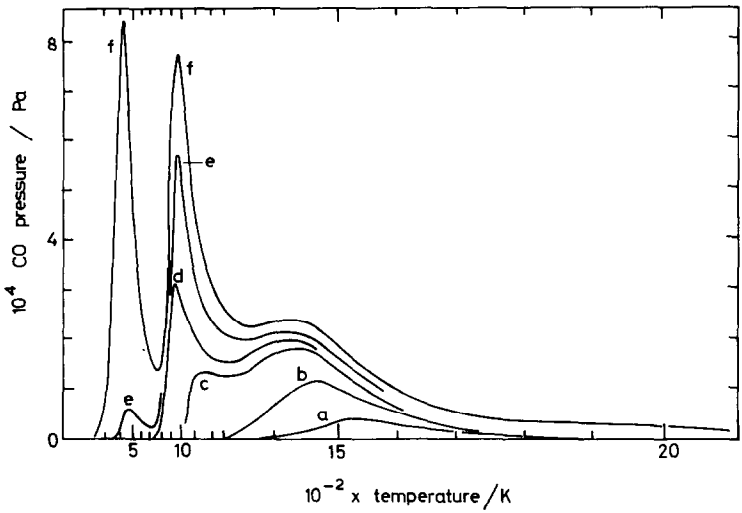

Fig. 8. Desorption traces for carbon monoxide on a tungsten ribbon at an adsorption temperature of 300 K; curves (a)–(e) correspond to increasing CO exposures. The α state peak temperature is 450 K; the β_1 and β_2 peaks are at 1000 K and 1440 K, respectively. Reproduced from Goymour and King [50], with permission.

and thorough X-ray photoelectron study has been reported by Yates, Madey and Erickson [48]; their results for the O(1s) core level in CO on W are summarised in fig. 9. Different electron binding energies were found to be associated with each of the states virgin, α_1, α_2 and β, while no distinction could be ascertained between β_1 and β_2. Further, the O(1s) binding energy for β-CO was found to be the same as that for O_2 adsorbed on tungsten. These results support both the lateral interaction model for the β peaks and the dissociative nature of the β state. However, we note that (a) indirect lateral interactions might be expected to cause a small chemical shift in the O(1s) level at high β-CO coverages, and (b) the authors themselves prefer a model in which there is some residual direct bonding between neighbouring C and O atoms. The latter problem has not been resolved by recent field emission energy distribution [49] or ultraviolet photoelectron [31,56] studies of the valence energy levels; thus Plummer concludes [31] that "β-CO has both the oxygen and carbon in intimate contact with the tungsten surface, with the tungsten–carbon and tungsten–oxygen bonds producing the predominant features of the CO spectrum, yet the C and O still interact either directly or indirectly via the substrate".

Goymour and King [8] applied the interaction model to the β state desorption traces on the assumption that the species is dissociated, deriving a repulsive interaction energy of 20 kJ mol^{-1}. The model was extended to cover a variable O:C ratio, and the computed spectra are again in good agreement with O_2/CO coadsorption

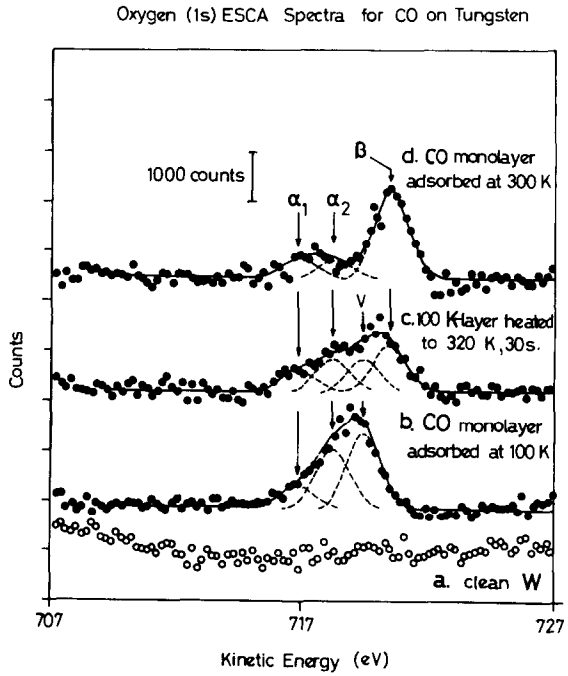

Fig. 9. X-ray photoelectron spectroscopy study of CO adsorption on a tungsten ribbon: the O (1s) core level spectra. Reproduced from Yates, Madey and Erickson [48], with permission.

results [57]. In particular, for O : C ratios above unity the model predicted an initial attenuation of the β_2 peak, which was observed experimentally. However, Adams [9] has applied the interaction model to thermal desorption data for CO on W{210} assuming non-dissociative adsorption in the β-state. He reports a reasonable description of the data with a coverage-dependent repulsive interaction energy of $(10.5 + 29\,\theta)\,\mathrm{kJ\,mol^{-1}}$.

6. Conclusion

Many further systems could be presented to illustrate the rich complexity of thermal desorption from metal surfaces. For example, desorption traces from oxygen on tungsten, which desorbs as O atoms and a range of oxides [10,58], point to a problem not discussed here: the effect of extensive substrate reconstruction on thermal desorption. The CO on Pd{100} system illustrates a form of interaction between adsorbed molecules, also not touched on here: in this case an in-registry–out-of-registry transition occurs at a half-monolayer coverage, with a consequential

discontinuous change in the differential adsorption energy [59,60]. Finally, the $N_2/W\{100\}$ system is one in which the simple-lateral interaction model for both desorption [9] and adsorption [27] kinetics appears to apply.

There exists a strong interrelationship between kinetics and all aspects of structure in adsorption. While we have stressed here that the former cannot be fully analysed in the absence of a complete understanding of the latter, it is equally true that thermal desorption studies have played, and will continue to play, a key role in developing our understanding of adsorbate structure.

Acknowledgement

Helpful discussions with Dr. J.W. Earnshaw during the preparation of the manuscript are gratefully acknowledged.

References

[1] L. Apker, Ind. Eng. Chem. 40 (1948) 846.
[2] G. Ehrlich, Advan. Catalysis 14 (1963) 255; J. Appl. Phys. 32 (1961) 4.
[3] P.A. Redhead, Vacuum 12 (1962) 203.
[4] P.A. Redhead, J.P. Hobson and E.V. Kornelsen, The Physical Basis of Ultrahigh Vacuum (Chapman and Hall, London, 1968).
[5] D.L. Adams, L.H. Germer and J.W. May, Surface Sci. 22 (1970) 45.
[6] R.R. Rye and B.D. Barford, Surface Sci. 27 (1971) 667.
[7] T. Toya, J. Vacuum Sci. Technology 9 (1972) 890; and personal communication.
[8] C.G. Goymour and D.A. King, J. Chem. Soc. Faraday I 69 (1973) 749.
[9] D.L. Adams, Surface Sci. 42 (1974) 12.
[10] D.A. King, T.E. Madey and J.T. Yates, J. Chem. Phys. 55 (1971) 3236.
[11] L.D. Schmidt, in: Adsorption–Desorption Phenomena, Ed. F. Ricca (Academic Press, London, 1972) p. 391; also, refs. 28, 35, 39 and 55.
[12] For example, refs. 13, 18, 29, 34 and 43.
[13] M.J. Dresser, T.E. Madey and J.T. Yates, Surface Sci. 42 (1974) 533.
[14] F.M. Lord and J.S. Kittelberger, Surface Sci. 43 (1974) 173.
[15] W.L. Winterbottom, J. Vacuum Sci. Technology 9 (1972) 936.
[16] W.L. Winterbotton, Surface Sci. 36 (1973) 195.
[17] C. Pisani, G. Rabino and F. Ricca, Surface Sci. 41 (1974) 277.
[18] J.T. Yates and T.E. Madey, J. Chem. Phys. 54 (1971) 4969.
[19] T.B. Grimley, Proc. Phys. Soc. (London) 90 (1967) 751.
[20] T.B. Grimley, Proc. Phys. Soc. (London) 92 (1967) 776.
[21] T.L. Einstein and J.R. Schrieffer, Phys. Rev. 87 (1973) 3629.
[22] T.B. Grimley and M. Torrini, J. Phys. C (Solid State Phys.) 6 (1973) 868.
[23] J.K. Roberts, Some Problems in Adsorption (Cambridge University Press, 1939).
[24] J.S. Wang, Proc. Roy. Soc. (London) A161 (1937) 127.
[25] J.S. Wang, Proc. Cambridge Phil. Soc. 34 (1938) 238.
[26] J. Hijmans and J. de Boer, Physica 21 (1955) 471.
[27] D.A. King and M.G. Wells, Proc. Roy. Soc. (London) A339 (1974) 245.

[28] P.W. Tamm and L.D. Schmidt, J. Chem. Phys. 54 (1971) 4775.
[29] T.E. Madey, Surface Sci. 36 (1973) 281.
[30] K.J. Matysik, Surface Sci. 29 (1972) 324.
[31] E.W. Plummer, in: Proc. of Hindas (Gothenberg) Conf., Sweden, 1973.
[32] D.A. King and D. Menzel, Surface Sci. 40 (1973) 399.
[33] T.L. Hill, Statistical Mechanics (McGraw-Hill, New York, 1956).
[34] T.E. Madey and J.T. Yates, in: Structure et Propriétés des Surface des Solides (CNRS, Paris, 1970) No. 187, p. 155.
[35] P.W. Tamm and L.D. Schmidt, J. Chem. Phys. 51 (1969) 5352; 52 (1970) 1150.
[36] F.M. Propst and T.C. Piper, J. Vacuum Sci. Technology 4 (1967) 53.
[37] E.W. Plummer and A.E. Bell, J. Vacuum Sci. Technology 9 (1972) 583.
[38] P.J. Estrup and J. Anderson, J. Chem. Phys. 45 (1966) 2254.
[39] K. Yonehara and L.D. Schmidt, Surface Sci. 25 (1971) 238.
[40] M.R. Leggett and R.A. Armstrong, Surface Sci. 24 (1971) 404.
[41] B.J. Waclawski and E.W. Plummer, Phys. Rev. Letters 29 (1972) 783.
[42] B. Feuerbacher and B. Fitton, Phys. Rev. Letters 29 (1972) 786.
[43] T.E. Madey, Surface Sci. 29 (1972) 571.
[44] D.A. King and M.G. Wells, Surface Sci. 29 (1972) 454.
[45] R.R. Ford, Advan. Catalysis 21 (1970) 51.
[46] D.A. King, C.G. Goymour and J.T. Yates, Proc. Roy. Soc. (London) A331 (1972) 361.
[47] D.L. Adams and L.H. Germer, Surface Sci. 32 (1972) 205.
[48] J.T. Yates, T.E. Madey and N.E. Erickson, Surface Sci. 43 (1974) 257.
[49] P.L. Young and R. Gomer, J. Chem. Phys., in press.
[50] C.G. Goymour and D.A. King, J. Chem. Soc. Faraday I 69 (1973) 736.
[51] T.E. Madey, J.T. Yates and R.C. Stern, J. Chem. Phys. 42 (1965) 1372.
[52] D. Menzel, Ber. Bunsenges. Physik. Chem. 72 (1968) 591.
[53] J.T. Yates and D.A. King, Surface Sci. 32 (1972) 479.
[54] J.T. Yates, R.G. Greenler, I. Ratajczykowa and D.A. King, Surface Sci. 36 (1973) 739.
[55] L.R. Clavenna and L.D. Schmidt, Surface Sci. 33 (1972) 11.
[56] J.M. Baker and D.E. Eastman, J. Vacuum Sci. Technology 10 (1973) 223.
[57] C.G. Goymour and D.A. King, Surface Sci. 35 (1973) 246.
[58] D.A. King, T.E. Madey and J.T. Yates, J. Chem. Phys. 55 (1971) 3247.
[59] J.C. Tracy and P.W. Palmberg, J. Chem. Phys. 51 (1969) 4852.
[60] G. Ertl, Surface Sci. 47 (1975) 86.